ChemSusChem

Research Article
doi.org/10.1002/cssc.202300932

Chemistry Europe
European Chemical Societies Publishing

www.chemsuschem.org

VIP *Very Important Paper*

# Long Cycle-Life Ca Batteries with Poly(anthraquinonylsulfide) Cathodes and Ca–Sn Alloy Anodes

Daniel Bier,[a, b] Zhenyou Li,*[a, c] Svetlana Klyatskaya,*[b] Najoua Sbei,[b] Ananyo Roy,[a] Sibylle Riedel,[a] Maximilian Fichtner,[a, b] Mario Ruben,*[b, d, e] and Zhirong Zhao-Karger*[a, b]

Calcium (Ca) batteries are attractive post-lithium battery technologies, due to their potential to provide high-voltage and high-energy systems in a sustainable manner. We investigated herein 1,5-poly(anthraquinonylsulfide) (PAQS) for Ca-ion storage with calcium tetrakis(hexafluoroisopropyloxy)borate $Ca[B(hfip)_4]_2$ [hfip = $OCH(CF_3)_2$] electrolytes. It is demonstrated that PAQS could be synthesized in a cost-effective approach and be processed environmentally friendly into the electrodes. The PAQS cathodes could provide 94 mAh $g^{-1}$ capacity at 2.2 V vs. Ca at 0.5C (1C = 225 mAh $g^{-1}$). However, cycling of the cells was severely hindered due to the fast degradation of the metal anode. Replacing the Ca metal anode with a calcium-tin (Ca–Sn) alloy anode, the PAQS cathodes exhibited long cycling performance (45 mAh $g^{-1}$ at 0.5C after 1000 cycles) and superior rate capability (52 mAh $g^{-1}$ at 5C). This is mainly ascribed to the flexible structure of PAQS and good compatibility of the alloy anodes with the electrolyte solutions, which allow reversible quinone carbonyl redox chemistry in the Ca battery systems. The promising properties of PAQS indicate that further exploration of the organic cathode materials could be a feasible direction towards green Ca batteries.

## Introduction

Since the early 1990s, lithium-ion batteries (LIBs) have become the most common choice for powering portable electrical devices, and soon penetrated into other fields of application. However, the explosive expansion of the LIB market raised concerns about the long-term availability of key raw materials required for this technology, such as cobalt, nickel and lithium (Li).[1] To meet the exponential market growth and diversified application scenarios, post-Li battery technologies with higher sustainability, lower cost, and better safety are in urgent demand. Among them, calcium (Ca)-based batteries emerged as one of the most promising candidates, due to the Earth abundance and low reduction potential of Ca. Ca is the fifth most abundant metal in the Earth's crust (4.1 %) making it 20 to 40 times cheaper compared to Li.[2] In addition, the reduction potential of Ca (−2.87 V vs. SHE) is comparable to Li (−3.04 V vs. SHE), showing the potential of building high-voltage and high-energy full-cells. Furthermore, $Ca^{2+}$ has larger ionic radius than other multivalent charge carriers, therefore with smaller charge density, which renders faster kinetics.

One major issue that hinders the development of Ca batteries is the incompatibility between the metal anode and non-aqueous electrolyte, similar as magnesium batteries.[3] Metallic Ca anode readily reacts with conventional aprotic solvents, forming a surface passivating film,[4] which allows the transport of $Ca^{2+}$ only at elevated temperature.[5] Calcium borohydride in tetrahydrofuran [$Ca(BH_4)_2$/THF] is the first electrolyte enabling reversible Ca plating/stripping at room temperature, however, with anodic stability only up to 3 V vs. Ca.[6] To enlarge the electrochemical window, we proposed to introduce weakly coordinating anions, which led to the development of a calcium tetrakis(hexafluoroisopropyloxy)borate ($Ca[B(hfip)_4]_2$) electrolyte.[7] A 0.25 M $Ca[B(hfip)_4]_2$/DME (DME = dimethoxyethane) electrolyte provided high ionic conductivity of

[a] D. Bier, Dr. Z. Li, A. Roy, Dr. S. Riedel, Prof. M. Fichtner, Dr. Z. Zhao-Karger
Helmholtz Institute Ulm (HIU)
Helmholtzstr. 11, D-89081 Ulm (Germany)
E-mail: zhenyou.li@kit.edu
zhirong.zhao-karger@kit.edu

[b] D. Bier, Dr. S. Klyatskaya, Dr. N. Sbei, Prof. M. Fichtner, Prof. M. Ruben, Dr. Z. Zhao-Karger
Institute of Nanotechnology (INT)
Karlsruhe Institute of Technology (KIT)
P.O. Box 3640, D-76021 Karlsruhe (Germany)
E-mail: svetlana.klyatskaya@kit.edu
mario.ruben@kit.edu

[c] Dr. Z. Li
Qingdao Institute of Bioenergy and Bioprocess Technology (QIBEBT)
Chinese Academy of Sciences
No. 189 Songling Road, Laoshan District, Qingdao, Shandong 266101 (China)

[d] Prof. M. Ruben
Institute for Quantum Materials and Technology (IQMT)
Karlsruhe Institute of Technology (KIT)
P.O. Box 3640, D-76021 Karlsruhe, Germany

[e] Prof. M. Ruben
Institut de Science et d'Ingénierie Supramolaiculaires (ISIS-CESQ)
Université de Strasbourg
Strasbourg Cedex F-67083, France

Supporting information for this article is available on the WWW under https://doi.org/10.1002/cssc.202300932

8 mS cm$^{-1}$ and high oxidative stability of 4 V. Despite the progresses, detrimental side reactions were found along with Ca deposition, which resulted in low efficiency and limited cyclability of the metal anode. As metallic Ca was problematic, alternative anodes, primarily alloy anodes, were brought to light.[8] Among them, Ca–Sn alloys exhibited so far the best performance.[9] Reversible calcination of tin (Sn) was reported with the formation of $Ca_7Sn_6$, which enabled long-term cycling of Ca-based dual-ion batteries.[9a] Inspired by that, we developed Ca-rich $Ca_xSn$ alloys for Ca batteries . By coupling the $Ca_xSn$ alloy anode with an organic cathode, the cell could be cycled for > 5000 times.[9b] By improving the anode-electrolyte compatibility, the exploration of high-performance electrolyte together with the alloy anodes paves the way to the investigation of viable cathodes for Ca-based batteries.

In search for suitable hosts, it is realized that the large ionic size and double charge of $Ca^{2+}$ hinders the reversible intercalation into rigid inorganic materials. Except for a few framework structures (e.g., Prussian blue analogues,[10] $FePO_4$[11] and NASICON compounds[12]), most of the investigated inorganic cathodes show poor Ca-ion storage performance. In contrast, organic compounds provide softer molecular structures, which could accommodate $Ca^{2+}$ more flexibly and thereby rendering faster ion mobility. Till now, only limited number of organic cathodes have been investigated for the storage of $Ca^{2+}$, most of them being redox-active polymers.[9b,13] This is because the redox-active polymers are capable of providing a relative stable redox potential, but also alleviating the leaking of active species into the electrolyte, which is a common issue for organic small molecules.

In our recent work, we evaluated polyanthraquinone (PAQ)-based composites as cathode materials for Ca batteries. When coupled with the $Ca_xSn$ alloy anode, the PAQ cathode exhibited a capacity retention of 78 mAh g$^{-1}$ after cycling at 1C (260 mA g$^{-1}$) for 5000 cycles.[9b] Inspired by these findings, we further developed a poly(anthraquinonylsulfide) (PAQS) cathode for Ca-based batteries in this work. Similar as the PAQ cathode, PAQS with redox-active carbonyl groups can offer a theoretical capacity of 225 mAh g$^{-1}$. In addition, PAQS can be synthesized from cheaper raw materials, which is beneficial for reducing the cost of the cells. The PAQS cathodes were previously investigated in a model cell configuration applying a capacitive carbon as counter electrode,[14] and later studied in quasi-full-cell Ca-organic batteries.[13b] However, due to the passivation issues of Ca metal anode, the Ca-PAQS cells could only be cycled for less than 10 times.

To improve the electrochemical performance of PAQS with a practical cell configuration, we applied herein the $Ca_xSn$ alloy anode as a replacement to the Ca metal anode. The alloy anode ensures a stable reversible redox reaction at the anode side, which allows appropriate evaluation of the PAQS cathodes. Therefore, the preparation and characterization of the $Ca_xSn$ as well as PAQS were carried out first. Subsequently, electrode formulation of PAQS was investigated targeting at a green processing method to prepare homogeneous coatings with desired mass loading. Based on that, the PAQS cathodes were electrochemically studied against Ca metal anode and the alloy anode, respectively. By using the $Ca_xSn$ anode, the optimized PAQS electrode provided a capacity of 45 mAh g$^{-1}$ at 0.5C (1C = 225 mA g$^{-1}$) after 1000 cycles.

## Results and Discussion

### Preparation and characterization of $Ca_xSn$ Alloy

$Ca_xSn$ alloy was prepared via a solid-state synthetic approach as reported previously,[9b] and was characterized by X-ray diffraction (XRD) analysis. In Figure 1, the XRD pattern of the as-prepared alloy shows main diffraction peaks at 13.6°, 15.1°, 16.1° and 17.0° corresponding to the (211), (013), (020) and (004) planes of the orthorhombic $Ca_2Sn$ structure, respectively. In addition to the Zintl phase $Ca_2Sn$, minor phases of CaSn and $Ca_{31}Sn_{20}$ were also identified.[15] Hence, the as-prepared alloy was denoted as $Ca_xSn$ in the following discussion. Overall, the XRD pattern revealed no traces of unreacted Ca and/or Sn powder indicating a full conversion of the reactants with 95.3% yield.

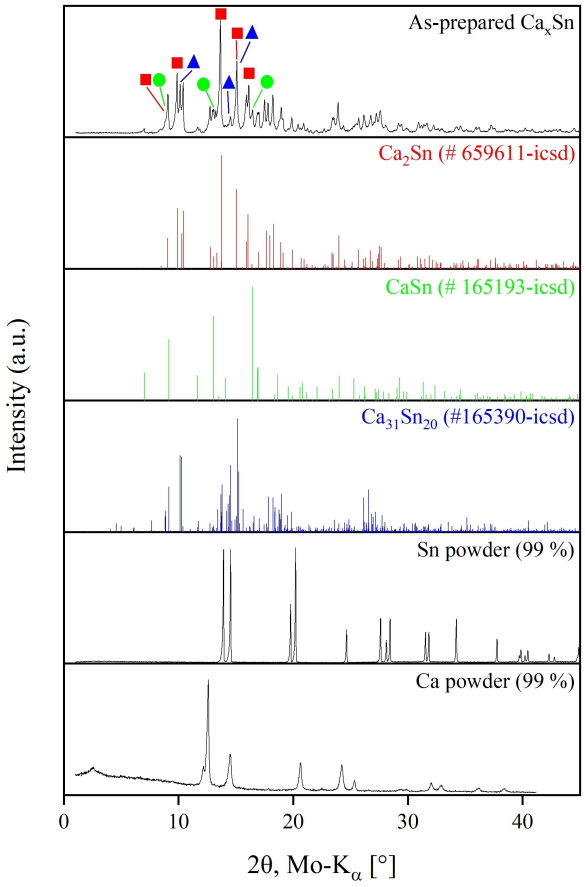


**Figure 1.** XRD patterns of the as-prepared $Ca_xSn$ alloy and its comparison with some reference patterns. Labels with different colour indicate peaks assigned to the respective major phases.

### Preparation and characterization of PAQS

1,5-PAQS was synthesized by a simple condensation reaction based on published procedure of Flamme et al.[16] with some modifications (see SI). The structure of the product was analyzed by attenuated total reflection infrared spectroscopy (ATR-IR) and Raman spectroscopy. The ATR-IR spectra in Figure 2b confirmed the conversion of 1,5-dichloroanthraquinone (DCAQ) by the weakening of the C–Cl band at 808 $cm^{-1}$.[17] Analog to 1,5-DCAQ, aromatic C=C stretching at around 1430 $cm^{-1}$ as well as one vibrational carbonyl band at 1680 $cm^{-1}$ correspond to the antharaquinoyl moiety. However, as the S grafted to the aromatic ring, the ring stretching shifted to lower wavenumbers. (see Figure 2a).[18]

In order to check if polysulfide moieties formed within the polymer structure, Raman spectroscopy was performed with a 532 nm laser from 1500 to 600 $cm^{-1}$. Figure 2c presents the Raman spectrum of the 1,5-PAQS in reference to 1,5-DCAQ and elemental sulfur. The spectrum shows only broad signals between 400 and 550 $cm^{-1}$ without clear bands associated with polysulfides, suggesting a structure free of S–S bonds.[19] In addition, elemental analysis of the product in Table S1 revealed an atomic ratio of C:H:N close to the theoretical stoichiometry of PAQS ($C_{14}H_6O_2S$), further confirming the successful synthesis of 1,5-PAQS.

To determine the polymerization degree of the synthesized polymers, matrix-assisted laser desorption/ionization-time of flight mass spectroscopy (MALDI-TOF MS) was performed using 3,5-dimethoxy-4-hydroxycinnamic acid (sinapinic acid) as matrix. It is worth mentioning that the solubility of PAQS was low and therefore the spectra were recorded at different acceleration voltages to ensure the best possible result. The spectra and a schematic of possible mass fragments can be found in Figure S1 and Figure S2, respectively. Because Cl being a good leaving group, the C–Cl breaks first in the initiation step forming phenyl radical derivates in the process. In the following chain propagation, C–Cl as well as C–S bonds are going to break forming different fragments with different m/z ratios. In addition, the dissociation of C–O bonds can be observed forming $C_{14}H_6S^{+\bullet}$ in the process. Throughout these experiments traces of Li can be found in all spectra. The origin of the Li can be explained by the residues of the educts during sample preparation. As shown in Figure S1, the main peak at 996.8 *m/z* could be assigned to $[(C_{14}H_6O_2S)_4\text{–}Li]^{+\bullet}$, indicating an average polymerization degree of $n = 4$. However, peaks at 758.8, 510.8, and 329.9 m/z also confirmed the formation of shorter polymers ($n = 1$–3). On the other hand, weak signals at 1236.8 *m/z* $[Cl\text{–}(C_{14}H_6O_2S)_5\text{–}Li]^{+\bullet}$ and 1253.78 *m/z* $[Cl\text{–}(C_{14}H_6S)_{12}]^{2+\bullet}$ indicate a small concentration of molecules with higher polymerization degrees ($n > 4$). Since MALDI sample preparation requires high solubility of analyte and matrix molecules and followed up co-crystallization,[20] the insolubility of giant polycyclic aromatic hydrocarbons (PAQS can be attributed to that class of organic material too) limits their characterization by this method to relatively low molecular weights (~2000), in the case of PAHs.[21] On those reasons, the values in MALDI-TOF we have achieved are a rough estimate only of the chain length.

To further investigate the polymerization degree of the PAQS, scanning electron microscopy with energy-dispersive X-ray spectroscopy (SEM-EDX) was applied. A typical SEM image of PAQS in Figure 3 showed an average particle size of around 1–2 µm. Some of the particles were agglomerated to bigger ones. The polymerization degree of PAQS can be determined by the atomic ratio of S/Cl. This is because Cl should theoretically only appear at both ends of the polymer chains,

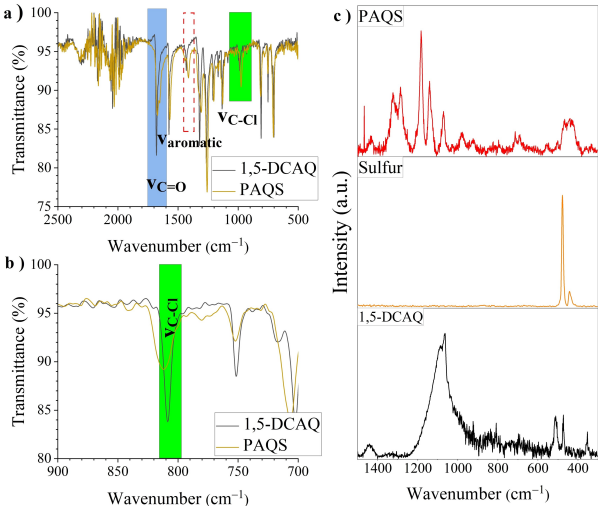


**Figure 2.** Spectroscopic analysis of the 1,5-PAQS polymer: (a) ATR-IR spectra compared to DCAQ monomer (black), (b) zoomed region between 700–900 $cm^{-1}$, (c) Raman spectrum of the 1,5-PAQS at 532 nm laser from 1500 to 600 $cm^{-1}$.

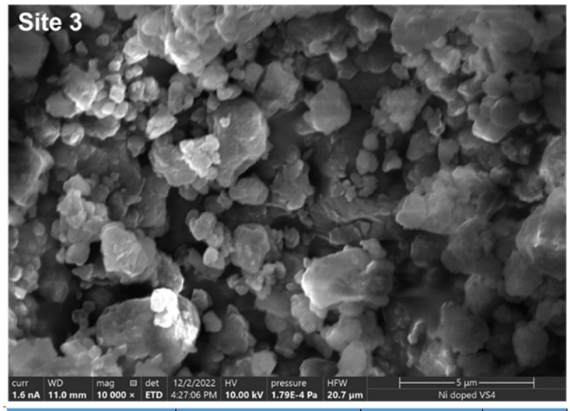


| Spectrum | Atomic % | | S/Cl ratio | n |
|---|---|---|---|---|
| | S | Cl | | |
| Site 1 | 10 | 1.5 | 6.6 | 12.3 |
| Site 2 | 4.3 | 1.8 | 2.3 | 3.7 |
| Site 3 | 25.7 | 3.5 | 7.3 | 13.6 |
| Site 4 | 11.8 | 1.7 | 6.9 | 12.8 |
| Site 5 | 11.6 | 1.7 | 6.8 | 12.6 |

**Figure 3.** Top: a typical SEM image of the PAQS. Bottom: atomic percentages of the PAQS at different measured sites, determined from EDX.

and each repeating unit contains one S. The detailed calculation method was given in Note S1 in the SI. According to the EDX data in Figure 3, an average polymerization degree of PAQS was determined to be around 12.

### Optimization of the cathode formulation

To better study the redox behaviors of PAQS in the presence of $Ca^{2+}$, cathode formulation was optimized. Slurries with different carbons, binders, solvent contents, and coating thicknesses were investigated to identify the electrode coating with the most favorable properties in terms of mass loading, homogeneity, and electrochemical performance. For the electrochemical tests, PAQS cathodes coupled with Ca metal anodes were cycled at 0.5C (1C = 225 mA $g^{-1}$) in the voltage range from 1.3 to 3.3 V.

Polymer cathodes generally suffer from swelling issue when in contact with solvent. As a result, different binders and mixing solvents were compared in the first set of experiments (see Figure 4a). Additionally, applying greener binder and non-toxic solvent could further enhance the sustainability of the PAQS-based polymer cathodes. As a benchmark, electrodes with polyvinylidene fluoride (PVDF) as binder, which are widely used in the literature, were investigated.[14,16,19,22] The electrode preparation was orientated on the work of Phadke et al.[22b] Here, PAQS, Ketjen Black EC JD-600 (KB), and PVDF were mixed in a mass ratio of 6:3:1 in N-Methyl-2-pyrrolidone (NMP) and coated with 400 μm thickness. The resultant electrode (B11) showed an initial discharge capacity of 55 mAh $g^{-1}$ and quickly reached their maximum capacity of 93 mAh $g^{-1}$ in the 3rd cycle followed by a rapid capacity loss between the 6th and 8th cycle. The sudden capacity drop could be attributed to the passivation of Ca metal anode, as previously reported.[13b] However, the PVDF-based coatings showed severe agglomeration, leading to large capacity deviation for electrodes with similar mass loading. In search for alternative binders, carboxymethyl cellulose (CMC) was tested, with a formulation of PAQS/AC/CMC (28.8:19.5:1 mass ratio, AC = activated carbon). The corresponding electrodes (B6) provided negligible initial capacity, which increased to ~28 mAh $g^{-1}$ (~12.7% theoretical capacity) after 15 cycles. The low capacity could be the result of a higher mass loading of the coating. Whereas the longer activation time indicated a less efficient wetting of the electrodes. Furthermore, PAQS cathodes with sodium alginate (SA) binder were also prepared, by suspending the active material with KB and 2.5 wt% SA solution in mass ratio of 6:3:1 in water. After mixing the slurry was coated with 300 μm thickness on carbon coted aluminum foil. The PAQS cathodes (B1) achieved an initial discharge capacity of 47 mAh $g^{-1}$ with Ca metal anodes. In the 6th cycle the cells reached their maximum of 80 mAh $g^{-1}$, which corresponded to 35.6% of the theoretical capacity (225 mAh $g^{-1}$). Compared with the electrodes using other binders, PAQS/KB/SA electrodes (B1) exhibited more homogeneous coating and has low environmental impact.

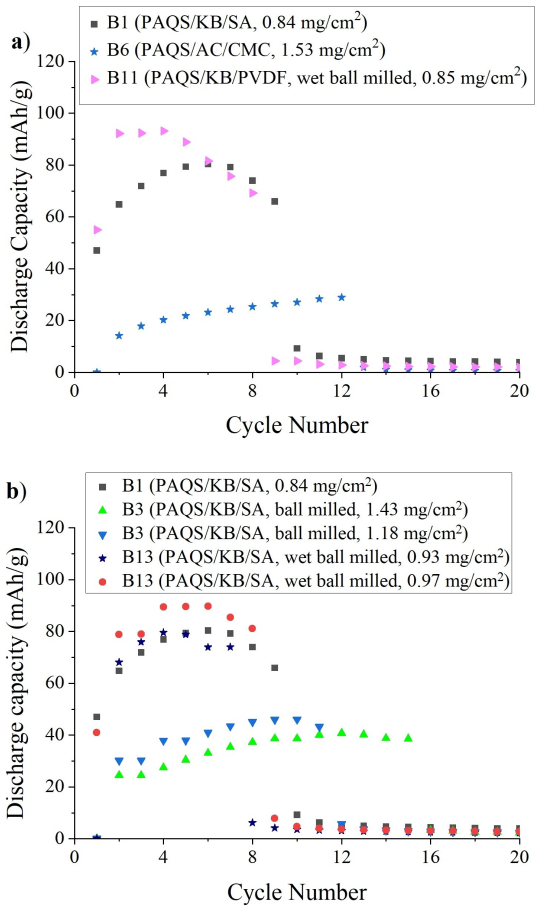


**Figure 4.** Optimization of the formulation of the PAQS-based cathodes, with specific parameters listed in Table S2. The screening was performed in coin cells with Ca metal anodes and cycled at 0.5C from 1.3 to 3.3 V. (a) Investigation of different conductive carbons and binders, (b) investigation of different electrode preparation methods.

Therefore, the subsequent trials were carried out focusing on PAQS with SA binder and KB, for further optimization. Although the initial PAQS/KB/SA coating (B1) showed relatively good electrochemical performance, the average mass loading was only ~0.5 mg $cm^{-2}$. Only 18.1% of the prepared electrodes (cut into Ø 13 mm discs) achieved an acceptable mass loading > 0.7 mg $cm^{-2}$. To increase the area loading, further optimization of the electrode composition was performed by investigating different slurry preparation methods as well as increasing the solvent content and thickness of the coating.

The solvent was adjusted for an optimized viscosity of the slurry. With a 6.65% of solid to liquid ratio, the PAQS/KB/SA coating (B8) showed an average mass loading slightly increased to 0.52 mg $cm^{-2}$ and 50% of the electrode discs > 0.7 mg $cm^{-2}$. Further decreasing the solid to liquid ratio to 5.07% (B14) led to a lower mass loading with 38% of the electrode discs > 0.7 mg $cm^{-2}$. To adjust the viscosity of the slurry, the water was replaced by an iPrOH/$H_2O$ mixture (1:3 *v/v*). By applying a coating thickness of 500 μm (wet thickness), the mass loading was increased to ~0.75 mg $cm^{-2}$, with 47.6% of the electrode discs > 0.7 mg $cm^{-2}$. The resultant PAQS cathode (B23) provided capacities between 80–90 mAh $g^{-1}$.

Targeting at a higher homogeneity of the coating, different processing methods of the electrode material were investigated

(Figure 4b). By ball milling PAQS and KB before the addition of the binder, a better mixing of the electrode materials was expected. However, ball milling did not increase the homogeneity of the coating in practice. Besides large mass differences, the average mass loading of the electrodes (B3) was only 0.47 mg cm$^{-2}$. In the battery tests, the ball-milled PAQS/KB/SA cathodes (B3) only achieved 46 mAh g$^{-1}$ maximum discharge capacity, which was only 50% of the untreated electrodes. A possible reason for that could be the high active material loss during the process. To counter this issue, wet milling was applied by adding small amount of ethanol (EtOH) to the solid mixture before ball milling. Then, the mortared material was dried overnight at 60 °C in a vacuum oven to completely remove EtOH. The resultant coating achieved a similar mass loading compared to the untreated material, with 58% of the electrodes discs reaching a mass loading of 0.7 mg cm$^{-2}$. Performance-wise, the wet ball milled cathodes (B13) showed similar capacities to the untreated electrodes, delivering a maximum capacity of 80–90 mAh g$^{-1}$, corresponding to ~40% of the theoretical value. One possible reason for the limited accessible capacity, when compared to the lithium system,[19,23] was the coordination environment provided by the PAQS structure. While $Li^+$ is a single charged cation that only coordinates to one C=O group, double charged $Ca^{2+}$ requires interaction with two neighboring redox-active centers, which leads to steric hindrance that limits the utilization of the C=O groups (Figure S8). Due to the reduced time and effort in electrode preparation, the untreated PAQS/KB/SA electrode preparation method (B22 or B23) was selected for all further electrochemical experiments.

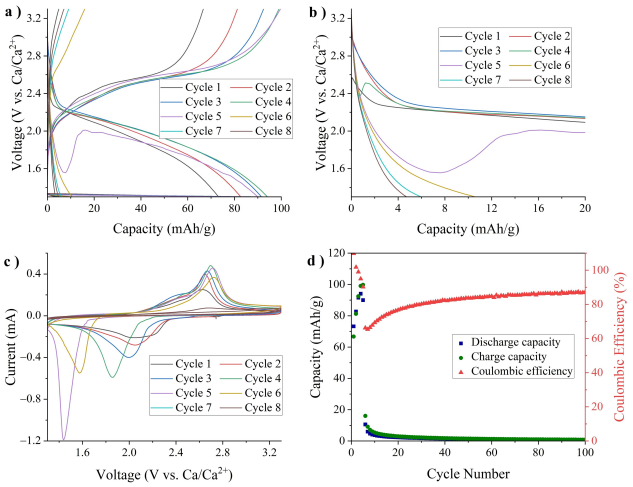


**Figure 5.** Electrochemical performance of the PAQS cathode vs. Ca metal anode. (a, b) Charge-discharge profile of the cathode cycled at 0.5C between 1.3 to 3.3 V. (c) CVs from 1.3 to 3.3 V at 0.5 mV s$^{-1}$. (d) Coulombic efficiency and capacities over cycle number.

## Electrochemical performance of the PAQS cathodes in Ca-based batteries

In all the electrochemical tests, a 0.25 M $Ca[B(hfip)_4]_2$/DME electrolyte was used. The chemical structure of the synthesized electrolyte compound was characterized by NMR as presented in Note S2 in the Supporting Information. While the electrochemical property of the electrolyte was confirmed by cyclic voltammetry (CV), applying a carbon-coated Al foil as working electrode and a Ca disc as counter electrode. The CVs in Figure S3 exhibited reversible Ca plating/stripping with Coulombic efficiency of ~80%, which is comparable with our previous report.[7]

As a benchmark, the PAQS cathodes were first tested against Ca metal anodes in the 0.25 M $Ca[B(hfip)_4]_2$/DME electrolyte at 0.5C. As shown in Figure 5a, the PAQS cathode delivered an initial capacity of 73 mAh g$^{-1}$, which was increased to 94 mAh g$^{-1}$ after 4 cycles. In the 5$^{th}$ cycle, a voltage dip appeared at the beginning of the discharge. And from the 6$^{th}$ cycle onwards, the voltage dip further developed (see Figure 5b), resulting in sudden decrease of the capacity (see Figure 5d). The increase of the voltage hysteresis indicated the degradation of Ca metal anode, which originated from partial decomposition of the electrolyte, leading to the formation of $CaF_2$ which impedes ionic transport. The increasing overpotential was also observed in the two-electrode CV profile. In Figure 5c, the first CV scan shows a reduction peak at 2.2 V with a shoulder peak at 2.0 V, and the corresponding oxidation peaks at 2.6 V and 2.4 V, respectively. The double redox pairs hint at a stepwise redox process between the C=O and C–O–,[9b] which might be due to the large size of $Ca^{2+}$. A similar profile was observed when testing PAQS cathodes in sodium ion batteries.[24] In the following cycles, the reduction peaks merged gradually into a single peak, while the oxidation peaks remained. This might indicate an activation of the polymer structure in the previous cycles for better accommodating $Ca^{2+}$. A mechanistic investigation of the carbonyl redox was carried out with ex-situ IR as presented in Figure S9 and discussed in Note S3. In addition, a drastic downshift of the reduction peak to 1.4 V and upshift of the oxidation peak to 2.7 V was evident, confirming the increasing anode overpotentials. The increase in overpotentials at the Ca anode is related to the enrichment of $CaF_2$ on the anode, which is associated with a sharp increase in polarization. The formation of $CaF_2$ together with the deposition of Ca metal has been observed in previous reports on the $Ca[B(hfip)_4]_2$-based electrolytes.[7,25] To overcome the limited cycling stability of Ca metal batteries, further development of organic electrolytes with higher stability to the metal anode is required. Another solution is to apply an alternative anode for Ca batteries.

Therefore, the PAQS cathodes were further investigated with the $Ca_xSn$ alloy anodes. Considering the redox potential of the alloy anode,[9b] the PAQS II 0.25 M $Ca[B(hfip)_4]_2$/DME II $Ca_xSn$ cells were investigated in a two-electrode set-up between 0.8 to 2.8 V. In Figure 6a, initial CV scans of the PAQS cathodes also show two redox pairs at 1.5 V/1.7 V and 1.3 V/1.5 V, which could be assigned to the conversion of C=O/C–O–. Compared to the cells with Ca metal anodes, the cells with the alloy anodes exhibited smaller hysteresis of 0.2 V for the overall redox process. Furthermore, there was only minor shifts of the redox peaks in the following cycles. These observations confirmed a

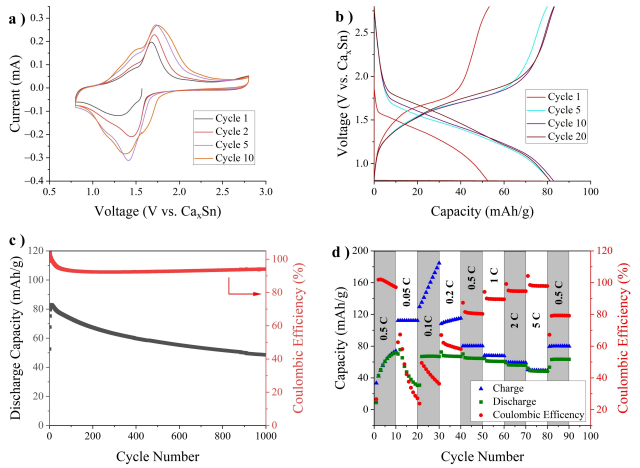


**Figure 6.** Electrochemical performance of the PAQS cathodes vs. $Ca_xSn$ alloy anodes: (a) CV at 0.5 mV $s^{-1}$ scan rate in the voltage range of 0.8 to 2.8 V; (b) voltage profiles of the cathode cycled at 0.5C; (c) discharge capacity and Coulombic efficiency over cycle number; (d) rate performance.

more stable anode process with a lower polarization. In addition, the small voltage hysteresis and its dependence on the applied anode suggested a highly reversible carbonyl redox at the cathode side. As for the galvanostatic cycling at 0.5C, the charge-discharge overpotential was also small as demonstrated in Figure 6b. The PAQS cathodes showed some activation cycles before reaching a maximum discharge capacity of 83 mAh $g^{-1}$, which was comparable to the test against a Ca metal anode. Impressively, the cycling stability significantly increased by using $Ca_xSn$ anode retaining 45 mAh $g^{-1}$ capacity after 1000 cycles (see Figure 6c). It was also noticed that there was overcharging in the initial cycles before the CE got stabilized. This could be related to the activation of the $Ca_xSn$ anode, with gradual formation of $CaSn_3$ as the new redox-active species.[9b]

On the basis of the long-term cycling stability, rate capability of the PAQS cathodes was further investigated. Due to the initial capacity increase, the cells were activated at 0.5C for 10 cycles as shown in Figure 6d. When cycling at 0.05C, 0.1C, 0.2C, 1C, 2C and 5C, the PAQS cathodes provided capacities of 70 mAh $g^{-1}$, 30 mAh $g^{-1}$, 72 mAh $g^{-1}$, 64 mAh $g^{-1}$, 59 mAh $g^{-1}$ and 52 mAh $g^{-1}$, respectively. Overall, a high capacity retention of 74% was achieved at 5C, demonstrating the fast-charging capability of the PAQS cathode. On the other hand, a drastic drop of Coulombic efficiency was evident at 0.05C accompanied by significant decreased discharge capacity. This is due to the experimental settings where a maximum charging time of 10 h was applied, to alleviate severe overcharging issue at lower C-rates. The overcharging issue became less prominent at higher C-rates, as evidenced by the increased Coulombic efficiencies. At the C-rates above 0.1C, the PAQS cathodes showed stable capacities, demonstrating highly reversible quinone carbonyl redox, which was consistent with the cycling data.

Overall, the PAQS cathodes exhibited excellent cycling stability and superior rate capability. PAQS can theoretically provide a capacity comparable to PAQ, and at a similar voltage, amounting to a similar specific energy. However, the synthesis of PAQ is costly as the C–C coupling reaction relies on zero-valent nickel-based catalysts, which are expensive.[26] Using S as a linker makes the polycondensation reaction easier. Therefore, the synthesis of PAQS is straightforward and requires only cost-efficient raw materials,[16] which makes it more attractive for practical applications. Further improving the performance of PAQS-based cathodes in Ca-based batteries might be achieved by cathode optimization to enhance the electronic conductivity and therefore higher utilization of the active materials. Another feasible approach could be to adjust the electrolyte formulation targeting any solubility issues. These strategies have been validated already in PAQ-based cathodes in both Mg-based and Ca-based batteries.[13b,14,27] However, as the use of high-surface area carbon leads to a lower energy density of the cathode, further optimization strategies should be developed to reduce the carbon content.

## Conclusions

The primary objective of this work was to evaluate poly(anthraquinonylsulfide) (PAQS) as a cathode material for $Ca^{2+}$ storage in practical cell configurations. In this context, PAQS was successfully synthesized with an average polymerization degree of ~12. Based on the as-prepared polymer, different electrode compositions were further investigated in order to have a homogeneous coating with desired loading. By applying sodium alginate (SA) as binder and iPrOH/$H_2O$ blend as mixing solvent, PAQS electrodes with an area mass loading of 0.75 mg $cm^{-2}$ were achieved. Replacing traditional polyvinylidene fluoride (PVDF)-N-Methyl-2-pyrrolidone (NMP)-based protocol by SA-iPrOH/$H_2O$ combination enhanced the sustainability of the electrode preparation. The resultant PAQS cathodes provided a capacity of 94 mAh $g^{-1}$ at 0.5C against Ca metal anodes, however, suffered from limited cycle life due to the fast degradation of the metal anodes. The cycle life of the cells was significantly improved by using $Ca_xSn$ alloy (mainly $Ca_2Sn$ phase) as alternative anodes, which allowed better and fair evaluation of the polymer cathode. In such cell configuration, the PAQS cathodes delivered a capacity of 83 mAh $g^{-1}$ at the same charging rate and could be cycled for 1000 times with a capacity retention of 45 mAh $g^{-1}$. Due to the flexible structure of the PAQS, the cathodes exhibited superior rate capability with a capacity of 52 mAh $g^{-1}$ at 5C. Overall, PAQS can be synthesized via a cost-efficient approach and the electrodes can be processed in an environmentally friendly manner, both of which rendering PAQS a promising cathode material for Ca-based batteries. As revealed by the mechanistic study, the electrochemical performance of PAQS could be further improved by enhancing the charge transfer e.g., using conductive matrix and/or allowing in-situ polymerization.

## Experimental Section

### Materials and methods

#### *Synthesis of $Ca_xSn$ alloy*

The synthesis of $Ca_xSn$ alloy was performed according to the paper of Zhao-Karger et al.[9b] All work steps were performed inside the glovebox ($H_2O < 0.9$ ppm, $O_2 < 2.3$ ppm). In a typical synthesis, 1.15 g calcium granules (28.69 mmol) and 1.48 g tin powder (12.80 mmol) were mixed in an aluminum oxide crucible. After sealing inside a quartz tube under argon atmosphere the mixture was heated up to 900 °C (100 °C $h^{-1}$ heating rate) and maintained the reaction temperature for 1 h. After cooling down to room temperature, the dark gray powder was mortared and stored under argon atmosphere. In the end, 2.54 g product (95.3 % yield) was obtained.

#### *Synthesis of 1,5-PAQS*

All the reactions were performed under Argon atmosphere using standard Schlenk techniques unless specified. All starting materials were purchased from commercial sources and were used as received. Solvents were freshly distilled over appropriate drying reagents.

The 1,5-PAQS was synthesized by a simple condensation reaction (Figure 7).[16] Instead of $Na_2S$, 0.83 g $Li_2S$ (18 mmol) was dissolved under argon atmosphere together with 4.99 g 1,5-DCAQ (18 mmol) in 40 mL NMP while stirring. The mixture was then heated to reflux at 200 °C for 48 h. After cooling to room temperature, the polymer was collected by centrifugation. The precipitate was thoroughly washed with water (3×200 mL) and acetone (3×100 mL) in order to remove unreacted $Li_2S$ and 1,5-DCAQ. The collected polymer was then dried under vacuum at 60 °C for 12 h. The product was obtained as a dark brown powder.

#### *Synthesis of $Ca[B(hfip)_4]_2 \cdot 4$ DME electrolyte*

The electrolyte was synthesized according to Li et al. under inert reaction condictions.[7] Under argon atmosphere 3.21 g $Ca(BH_4)_2 \cdot 2$ THF powder (15.0 mmol) was suspended into 60.0 mL DME in a two necked Schlenk flask equipped with a reflux condenser. Next 13.0 mL hexafluoroisopropanol (H-hfip) were slowly added dropwise to the solution while stirring (400 rpm, dropping speed ~5 drops/min). Then, the reaction mixture was refluxed at 85 °C for 4 h. After cooling down to room temperature the solvent was removed under vacuum. The raw product was further dried at 60 °C under vaccum *via* Büchi apparature at 6 rpm rotation overnight. At the end 22.46 g (85.5 % yield) of the product was obtained in the form of a white solid. The chemical structure of the product was confirmed by NMR spectroscopy as presented in Note S2 [$^1$H-NMR (500 MHz, THF-$d_8$) $\delta = 4.73$ ppm (m, CH), 3.43 ppm (s, DME-$CH_2$), 3.27 ppm (s, DME-$CH_3$); $^{19}$F - NMR (471 MHz, THF-$d_8$, H-decoupled) $\delta = 75.39$ ppm (s, $CF_3$); $^{11}$B-NMR (161 MHz, THF-$d_8$, H-decoupled) $\delta =$ 1.67 ppm].

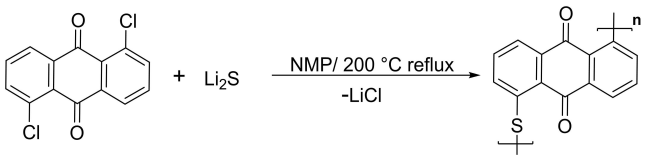


**Figure 7.** Synthesis of 1,5-PAQS.

#### *Electrode preparation*

The cathode material was prepared by suspending 0.120 g PAQS active material, 0.06 g hand milled Ketjen Black 600-JD as conductive carbon and 0.8 mL 2.5 wt % sodium alginate (aq) binder in 4.0 mL iPrOH/$H_2O$ (1 : 3 *v/v*). The slurry was prepared by mixing at 2000 rpm for 15 min followed by defoaming at 2200 rpm for 5 min, using a Thinky mixer. After 10 min rest the process was repeated. Then, the slurry was coated with 500 μm thickness on carbon coated Al foil. After drying under the fume hood for 5 h electrodes with 11.8 mm were prepared and further dried *via* Büchi at 80 °C under vacuum overnight. For electrochemical experiments PAQS electrodes with ~0.7 mg $cm^{-2}$ mass loading were used. As for the PAQS/KB/CMC electrodes 55.8 mg PAQS, 37.9 mg AC, and 0.1 mL 2.3 wt % CMC (aq) were mixed together with 3.4 mg super conductive C and 0.1 mL SBR (aq) as additives. An overview about the different electrode preparations in this work can be found in Table S2.

The Ca–Sn alloy anodes were prepared by mixing $Ca_xSn$ powder, KB, and polytetrafluoroethylene (PTFE) binder at a mass ratio of 6 : 3 : 1 in a FRITSCH P7 premium ball mill. Then, the mixture was hot-pressed at 87 °C onto a stainless-steel mesh by using a hydraulic press (10 MPa pressure, holding for 5 min). The formed alloy electrode had a diameter of 10 mm and an active mass loading of ~12 mg $cm^{-2}$.

As for the Ca metal anode Ca granules were hydraulic pressed to form pellets with ~12 mm in diameter.

### Electrochemical measurements

All electrochemical experiments were performed within stainless steel CR2032 type coin cell (20 mm diameter and 3.2 mm thickness) using PAQS cathodes (11.8 mm) coupled with either Ca metal (12 mm) or $Ca_xSn$ alloy anodes (10 mm). Two GF/C separators (16 mm) impregnated with 100 μL 0.25 M $Ca[B(hfip)_4]_2$/DME electrolyte separated the working electrode and counter electrode. The cells with Ca metal anodes were cycled between 1.3 and 3.3 V. While in case of $Ca_xSn$ anodes, a cut-off voltage range from 0.8 to 2.8 V was used. Battery tests with the GPCL technique were performed with a Biologic BCS-805 battery cycler. And CVs were recorded at a scan rate of 0.5 mV $s^{-1}$, applying a Biologic VMP-3 potentiostat.

### Characterizations

Crystal structure of the materials was confirmed by X-ray diffraction (XRD) with Mo-$K_\alpha$ radiation source ($\lambda = 0.709300$ Å) at 50 kV and 40 mA. NMR measurements of the $Ca[B(hfip)_4]_2 \cdot 4$ DME electrolyte were obtained by using a Bruker Advance II 500 spectrometer. The $^{11}$B-, $^{19}$F- and $^1$H-NMR spectra were collected using THF-d8 as solvent. Raman spectroscopy was performed by Via Raman microscope (RENISHAW). For sulfur, Ketjen Black EC 600-JD, and PAQS, spectra were collected with a 532 nm laser, 20× zoom, 10 s extinction time (Ex) and 1 % laser power (LP). As for 1,5-DCAQ the spectra were measured with a 785 nm laser excitation (1 % LP, 10 s Ex) and 20× zoom. Attenuated total reflection infrared spectroscopy (ATR-IR) was conducted by NICOLET iS50 ATR-IR (thermos scientific) as material characterization for PAQS. The *ex-situ* characterization of the PAQS cathodes was performed also under ATR mode but using a UATR spectrometer (Perkin Elmer). For *ex-situ* study, the cells were stopped at selected states of charge of the 3$^{rd}$ cycle. After disassembling inside the glove box ($H_2O = 0.6$ ppm, $O_2 = 0.6$ ppm), the cathode was washed 3×2 mL DME and dried in Büchi apparatus overnight at 80 °C under vacuum. SEM-EDX were recorded at 5 kV

using Apreo 2S from ThermoFisher Scientific equipped a ETD. The SEM images used at range between 50 pA to 100 pA while EDX was recorded at 1.6 nA. The evolution of the date was done by xT microscope Server with Microscope Control user interface (UI) software. The elemental analysis was conducted using a VARIO micro cube in CHNS-mode. MALDI-TOF MS experiments were performed using a Synapt G2-S HDMS MALDI-TOF/TOF MS according to the literature.[28] The sample was dissolved by immersion in a solution of acetic acid in ethanol (250 μL/0.2 mL). 0.5 μL of the resulting liquid was mixed with 0.5 μL of a matrix solution consisting of 5 mg of 3,5-dimethoxy-4-hydroxycinnamic acid (sinapinic acid) in 1 mL dichloromethane. Then, 0.5 μL of this mixture solution was spotted onto the MALDI target and air dried. The data acquisition was performed in reflector positive ion mode. As for the data analysis waters software was used.

## Supporting Information

The authors have cited additional references within the Supporting Information.[29]

## *Acknowledgements*

This work contributes to the research performed at CELEST (Center for Electrochemical Energy Storage Ulm-Karlsruhe) and was partly funded by the German Research Foundation (DFG) under Project ID 390874152 (POLiS Cluster of Excellence) and the Federal Ministry of Education and Research (Bundesministerium für Bildung und Forschung, BMBF) of Germany within the project "CaSino" (03XPO487E). Open access funding enabled and organized by Projekt DEAL. Open Access funding enabled and organized by Projekt DEAL.

## *Conflict of Interests*

The authors declare no conflict of interest.

## *Data Availability Statement*

The data that support the findings of this study are available from the corresponding author upon reasonable request.

**Keywords:** organic electrode · Ca–Sn alloy · calcium-based batteries · poly(anthraquinonylsulfide) · cycle life

[1] a) D. Larcher, J. M. Tarascon, *Nat. Chem.* **2015**, *7*, 19–29; b) J. W. Choi, D. Aurbach, *Nat. Rev. Mater.* **2016**, *1*, 16013; c) C. P. Grey, J. M. Tarascon, *Nat. Mater.* **2017**, *16*, 45–56.
[2] a) *Chemistry of the Elements (Second Edition)* (Eds.: N. N. Greenwood, A. Earnshaw), Butterworth-Heinemann, Oxford **1997**, pp. 107–138; b) L. Stievano, I. de Meatza, J. Bitenc, C. Cavallo, S. Brutti, M. A. Navarra, *J. Power Sources* **2021**, *482*, 228875.
[3] W. Ren, M. Cheng, Y. Wang, D. Zhang, Y. Yang, J. Yang, J. Wang, Y. NuLi, *Batteries & Supercaps* **2022**, *5*, e202200263.
[4] D. Aurbach, R. Skaletsky, Y. Gofer, *J. Electrochem. Soc.* **1991**, *138*, 3536.
[5] A. Ponrouch, C. Frontera, F. Bardé, M. R. Palacín, *Nat. Mater.* **2016**, *15*, 169–172.
[6] D. Wang, X. Gao, Y. Chen, L. Jin, C. Kuss, P. G. Bruce, *Nat. Mater.* **2018**, *17*, 16–20.
[7] Z. Li, O. Fuhr, M. Fichtner, Z. Zhao-Karger, *Energy Environ. Sci.* **2019**, *12*, 3496–3501.
[8] Z. Yao, V. I. Hegde, A. Aspuru-Guzik, C. Wolverton, *Adv. Energy Mater.* **2019**, *9*, 1802994.
[9] a) M. Wang, C. Jiang, S. Zhang, X. Song, Y. Tang, H.-M. Cheng, *Nat. Chem.* **2018**, *10*, 667–672; b) Z. Zhao-Karger, Y. Xiu, Z. Li, A. Reupert, T. Smok, M. Fichtner, *Nat. Commun.* **2022**, *13*, 3849; c) Y. Xiu, A. Mauri, S. Dinda, Y. Pramudya, Z. Ding, T. Diemant, A. Sarkar, L. Wang, Z. Li, W. Wenzel, M. Fichtner, Z. Zhao-Karger, *Angew. Chem. Int. Ed.* **2023**, *62*, e202212339.
[10] A. L. Lipson, B. Pan, S. H. Lapidus, C. Liao, J. T. Vaughey, B. J. Ingram, *Chem. Mater.* **2015**, *27*, 8442–8447.
[11] S. Kim, L. Yin, M. H. Lee, P. Parajuli, L. Blanc, T. T. Fister, H. Park, B. J. Kwon, B. J. Ingram, P. Zapol, R. F. Klie, K. Kang, L. F. Nazar, S. H. Lapidus, J. T. Vaughey, *ACS Energy Lett.* **2020**, *5*, 3203–3211.
[12] Z.-L. Xu, J. Park, J. Wang, H. Moon, G. Yoon, J. Lim, Y.-J. Ko, S.-P. Cho, S.-Y. Lee, K. Kang, *Nat. Commun.* **2021**, *12*, 3369.
[13] a) M. S. Chae, A. Nimkar, N. Shpigel, Y. Gofer, D. Aurbach, *ACS Energy Lett.* **2021**, *6*, 2659–2665; b) J. Bitenc, A. Scafuri, K. Pirnat, M. Lozinšek, I. Jerman, J. Grdadolnik, B. Fraisse, R. Berthelot, L. Stievano, R. Dominko, *Batteries & Supercaps* **2021**, *4*, 214–220.
[14] S. Zhang, Y. Zhu, D. Wang, C. Li, Y. Han, Z. Shi, S. Feng, *Adv. Sci.* **2022**, *9*, 2200397.
[15] a) H. Okamoto, *J. Phase Equilib.* **2001**, *22*, 589–590; b) A. Palenzona, P. Manfrinetti, M. L. Fornasini, *J. Alloys Compd.* **2000**, *312*, 165–171.
[16] B. Flamme, B. Jismy, M. Abarbri, M. Anouti, *Materials Advances* **2021**, *2*, 376–383.
[17] V. Krishnakumar, R. J. Xavier, *Spectrochim. Acta Part A* **2005**, *61*, 1799–1809.
[18] Z. Song, H. Zhan, Y. Zhou, *Chem. Commun.* **2009**, 448–450.
[19] I. Gomez, O. Leonet, J. Alberto Blazquez, H.-J. Grande, D. Mecerreyes, *ACS Macro Lett.* **2018**, *7*, 419–424.
[20] S. Trimpin, D. E. Clemmer, C. N. McEwen, *J. Am. Soc. Mass Spectrom.* **2007**, *18*, 1967–1972.
[21] L. Przybilla, J.-D. Brand, K. Yoshimura, H. J. Räder, K. Müllen, *Anal. Chem.* **2000**, *72*, 4591–4597.
[22] a) Z. Jian, Y. Liang, I. A. Rodríguez-Pérez, Y. Yao, X. Ji, *Electrochem. Commun.* **2016**, *71*, 5–8; b) S. Phadke, M. Cao, M. Anouti, *ChemSusChem* **2018**, *11*, 965–974.
[23] A. Vizintin, J. Bitenc, A. Kopač Lautar, K. Pirnat, J. Grdadolnik, J. Stare, A. Randon-Vitanova, R. Dominko, *Nat. Commun.* **2018**, *9*, 661.
[24] G. Ding, L. Zhu, Q. Han, L. Xie, X. Yang, L. Chen, G. Wang, X. Cao, *Electrochim. Acta* **2021**, *394*, 139116.
[25] A. Shyamsunder, L. E. Blanc, A. Assoud, L. F. Nazar, *ACS Energy Lett.* **2019**, *4*, 2271–2276.
[26] Z. Song, Y. Qian, M. L. Gordin, D. Tang, T. Xu, M. Otani, H. Zhan, H. Zhou, D. Wang, *Angew. Chem. Int. Ed.* **2015**, *54*, 13947–13951.
[27] a) Y. Xiu, Z. Li, V. Bhaghavathi Parambath, Z. Ding, L. Wang, A. Reupert, M. Fichtner, Z. Zhao-Karger, *Batteries & Supercaps* **2021**, *4*, 1850–1857; b) B. Pan, J. Huang, Z. Feng, L. Zeng, M. He, L. Zhang, J. T. Vaughey, M. J. Bedzyk, P. Fenter, Z. Zhang, A. K. Burrell, C. Liao, *Adv. Energy Mater.* **2016**, *6*, 1600140.
[28] S. Klyatskaya, A. B. Kanj, C. Molina-Jirón, S. Heidrich, L. Velasco, C. Natzeck, H. Gliemann, S. Heissler, P. Weidler, W. Wenzel, C. C. B. Bufon, L. Heinke, C. Wöll, M. Ruben, *ACS Appl. Mater. Interfaces* **2020**, *12*, 30972–30979.
[29] J. Bitenc, N. Lindahl, A. Vizintin, M. E. Abdelhamid, R. Dominko, P. Johansson, *Energy Storage Mater.* **2020**, *24*, 379–383.

Manuscript received: June 28, 2023
Revised manuscript received: July 31, 2023
Accepted manuscript online: August 1, 2023
Version of record online: ■■, ■■

# RESEARCH ARTICLE

**Organic electrode**: 1,5-poly(anthraquinonylsulfide) (PAQS) is evaluated as cathode material for calcium batteries. It is demonstrated that the practical performance of the PAQS cathode is governed by the employed anode. Replacing the Ca metal anode with a calcium-tin ($Ca_xSn$) alloy anode gave rise to significantly increased cycle life. With the as-prepared $Ca_xSn$ anode, the PAQS cathode could be cycled at 0.5C (1C = 226 mAh $g^{-1}$) for 1000 cycles with a capacity retention of 45 mAh $g^{-1}$.

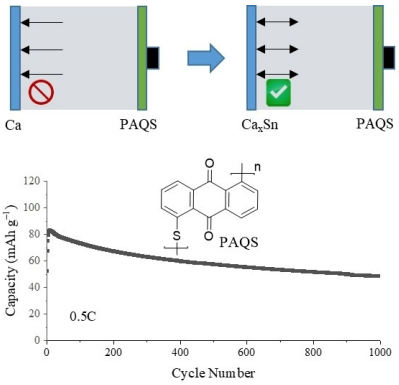


*D. Bier, Dr. Z. Li*, Dr. S. Klyatskaya*, Dr. N. Sbei, A. Roy, Dr. S. Riedel, Prof. M. Fichtner, Prof. M. Ruben*, Dr. Z. Zhao-Karger**